Proc. Indian Acad. Sci. (Earth Planet. Sci.), Vol. 96, No. 3, December 1987, pp. 279–290.

A steady state model of the Somali current

P K DAS, S K DUBE and G S RAO

Centre for Atmospheric Sciences, Indian Institute of Technology, New Delhi 110 016, India

MS received 30 November 1987

Abstract. A steady state model of the Somali current including forcing by both the curl and the divergence of the wind stress is discussed. The model equations are linear, but the results presented are for the one nonlinear case. The grid resolution was 12 km in the zonal and 24 km in the meridional direction. The streamfunction and velocity potential of the current are presented for forcing by divergence and compared with a situation when only the curl is present. The results indicate that a two-gyre system appears in July, a representative month for the summer monsoon, only when divergence is included. Computations with available data indicate that the divergence is comparable in magnitude to the curl near the location of the Somali current. The model produces three other important features: (i) strong upwelling off the east coast of Africa, (ii) downwelling over central Arabian sea and (iii) a strong eastward current in the upper layer towards the interior of the Arabian sea near 12°N.

Keywords. Somali current; curl; divergence; wind stress; upwelling; downwelling.

1. Introduction

A comprehensive investigation by Luther and O'Brien (1985) was able to simulate many features of the Somali current by a time-dependent model. Of particular interest was a two-gyre configuration beginning in June which ultimately coalesced towards the end of the summer monsoon. This result is interesting because Dube *et al* (1986) found that the southern gyre of the Somali current is prominent in a year of good monsoon, but is absent in a poor monsoon year.

The present paper suggests that an additional forcing by the divergence of the wind stress, in addition to the curl, leads to the formation of the second gyre.

2. Basic equations

We consider a two-layer ocean with an upper mixed layer and a deeper lower layer in which there is no motion. Turbulent mixing in the upper layer is sufficiently strong so that the wind stress acts as a body force throughout the depth of the mixed layer.

The wind induced current in the mixed layer is the sum of a rotational and a divergent part. Thus

$$\mathbf{V} = \hat{k} \times \nabla\psi + \nabla x, \tag{1}$$

where **V** is a depth-averaged current, $\hat{k}$ the unit vector along the vertical axis Z pointing upwards. ψ represents a streamfunction and x is a velocity potential for the wind-driven current. ψ and x will be determined by linearized equations for the conservation of vorticity and divergence.

Assuming a steady state and using the β-plane approximation for meridional variations of the Coriolis force f we have

$$-\beta y v = -\alpha \frac{\partial p}{\partial x} + \alpha \frac{\partial \tau_x}{\partial Z}, \tag{2}$$

$$\beta y u = -\alpha \frac{\partial p}{\partial y} + \alpha \frac{\partial \tau_y}{\partial Z}, \tag{3}$$

where α stands for the specific volume of water and $\beta = (\mathrm{d}f/\mathrm{d}y)$. In cartesian coordinates $(oxyz)$ u and v represent the zonal and meridional components of V and τ_x and τ_y are the components of the wind stress towards the east and north. The pressure p is related to the depth of the mixed layer h by

$$p = g'(h-H)\rho, \tag{4}$$

where $Z = -H$ is the mean undisturbed depth of the mixed layer. For a two-layer ocean, g' stands for the reduced gravity $[g(\Delta\rho/\rho)]$ in which $\Delta\rho$ is the difference in densities of the upper and lower layer and ρ is the density of the upper layer.

Integrating (2) and (3) from the surface ($Z = 0$) to the base of the mixed layer ($Z = -H$) we find

$$kU - \beta y V = -\alpha \frac{\partial p}{\partial X} + \frac{\alpha}{H}(\tau_x)_0 \tag{5}$$

$$kV + \beta y U = -\alpha \frac{\partial p}{\partial y} + \frac{\alpha}{H}(\tau_y)_0, \tag{6}$$

where the suffix 0 denotes the values of τ_x and τ_y at the surface. The depth-averaged components of the current are

$$U = \frac{1}{H}\int_{-H}^{0} u\,\mathrm{d}Z, \tag{7}$$

$$V = \frac{1}{H}\int_{-H}^{0} v\,\mathrm{d}Z. \tag{8}$$

Following Stommel (1948), we have assumed that the frictional stress at the interface between the mixed layer and the deeper ocean below is proportional to U, V. We have put

$$\alpha\tau_x = \sigma U, \tag{9}$$

$$\alpha\tau_y = \sigma V. \tag{10}$$

at $Z = -H$. k represents the ratio σ/H. Its value is not known with much precision, but its order of magnitude is $10^{-6}\mathrm{s}^{-1}$. We will use this value of k in our

Table 1. Orders of magnitude (s^{-2})

kD	βV	$\beta y\zeta$	$-\alpha\nabla_p^2$	$\frac{\alpha}{H}(\nabla\cdot\tau)_0$
10^{-12}	10^{-12}	$10^{-12}-10^{-11}$	10^{-11}	10^{-11}

computations. An experiment was performed with $k = 2\times10^{-6}s^{-1}$, but the results did not show any significant change.

From (2) and (3), the vorticity ζ and the divergence D is given by

$$k\zeta+\beta V+\beta yD = \frac{\alpha}{H}\hat{k}\cdot(\nabla\times\tau)_0, \tag{11}$$

$$kD + \underline{\beta u} - \underline{\beta y\zeta} = \underline{-\alpha\nabla^2 p} + \frac{\alpha}{H}(\nabla\cdot\tau)_0. \tag{12}$$

The underlined terms in (12) represent a geostrophic balance. Considering the representative values of vorticity and divergence to be $10^{-6}s^{-1}$, we find that the different terms of (12) have the orders of magnitude shown in table 1.

The third term ($\beta y\zeta$) has the magnitude shown in table 1 in the region within $\pm10°$ on either side of the equator. As shown subsequently, the available wind data suggest that the divergence is of comparable magnitude to the curl. Moreover, as we can see, the geostrophic balance is unlikely in the near equatorial regions where the Somali current is located. Consequently, it is necessary to include the effect of divergence in the model.

Equations (11) and (12) form a coupled system of two equations. As a first approximation, the barotropic response to the wind stress curl was computed without the stretching term (βyD) in (11). The resulting streamfunction ψ is determined by the equation

$$\nabla^2\psi + \left(\frac{\beta}{k}\right)\frac{\partial\psi}{\partial X} = \left(\frac{\alpha}{kH}\right)\hat{k}\cdot(\nabla\times\tau)_0. \tag{13}$$

with appropriate boundary conditions. This is Stommel's (1948) classical equation.

Similarly, a first approximation to the divergent part of the current is found by solving (12) without the second and third terms ($\beta u, \beta y\zeta$). We have

$$\nabla^2\phi = \frac{1}{H}(\nabla\cdot\tau)_0, \tag{14}$$

where

$$\phi = (k\rho x+p). \tag{15}$$

As $\nabla^2(k\rho x) > \nabla^2 p$ the solution of (14) provides a reasonably good estimate of the velocity potential x.

The velocity potential may be used to estimate the intensity of upwelling. Variations in h at the interface between the upper mixed layer and the deeper

ocean usually exceed similar variations at the surface ($Z = 0$). This is expressed by putting

$$W(-H) = \frac{\overline{\partial h}}{\partial t} = -H\nabla^2 x, \tag{16}$$

where an overbar indicates a mean value.

An estimate of vertical motion at the base of the mixed layer $[W(-H)]$ is thus provided by $\nabla^2 x$.

3. Successive approximations and boundary conditions

Equation (13) was first solved by relaxation over the region shown in figure 1. This was the first approximation to the streamfunction which will be referred to as ψ_0.

Similarly, solving (14) by relaxation provides the first approximation to the velocity potential. This is x_0.

Computing the Laplacian of x_0 provides a first estimate of divergence D_0. Inserting this in the stretching term (βyD) of (11) gives us a second approximation to the streamfunction, which is ψ_1. Similarly, the Laplacian of ψ_0 will provide an estimate of $\beta y\zeta$ in (12) and the solution of this equation gives us x_1.

A staircase pattern was adopted for land boundaries. Finite difference coordinates are defined by

$$X = (m-1)\Delta X, \ (m = 1,2.\ldots M) \tag{17}$$

$$Y = (n-1)\Delta Y, \ (n = 1,2.\ldots N),$$

where $\Delta X = 12$ km and $\Delta Y = 24$ km. The land boundaries are at $m = 1$, M and $n = 1$, N. An over-relaxation factor of 1·2 was found to be suitable for our purpose.

The boundary conditions are

$$\psi = \partial\psi/\partial n = 0$$

$$x = \partial x/\partial n = 0 \tag{18}$$

which provide no flux normal to the land boundaries. These conditions are not realistic along the open sea boundary to the south, but the currents measured by Cutler and Swallow (1984) during the monsoon indicate that along 10°S the flow is largely zonal and directed westwards. Thus, the absence of normal flux on the open boundary is not likely to influence the pattern of ψ and x in the interior of the region.

Results will be presented to indicate the streamline and velocity potential up to the second approximation. Computations for the third approximation were also made but are not reproduced here because it was found that, apart from an intensification of the gyres, there was no significant difference between the second and third approximations. This intensification in higher order approximations is largely brought about by the terms ($\beta yD, \beta y\zeta$) in (11) and (12). Increasing the distance y from the equator gives them an unreal dominance. Our main purpose, however, is to see how the divergence generated by $(\nabla\cdot\tau)_0$ in (12) leads to

additional vorticity by the stretching term in (11). This becomes clear even as we proceed from the first ψ_0 to the second approximation ψ_1 of the streamfunction.

It is possible, in principle, to eliminate divergence D from (11) and (12) and obtain a single equation for vorticity ζ. But this would have meant solving a higher order equation with mixed derivatives and more cumbersome boundary conditions. The use of successive approximations is simpler.

Nonlinear terms were not considered in the vorticity and divergence equations, but their effect may be inferred qualitatively. Here, it is convenient to express (13) in the form

$$J(\psi, \nabla^2\psi) + \beta V + \beta y D = \frac{\alpha}{H}\ \hat{k} \cdot (\nabla \times \boldsymbol{\tau})_0 - k\zeta, \tag{19}$$

where J stands for the Jacobian operator. Terms on the left of (19) represent (i) nonlinear advection of vorticity, (ii) meridional transport of planetary vorticity and (iii) vorticity generated by the stretching of vortex tubes, while on the right we express forcing by the curl and dissipation by interfacial friction. When additional vorticity is inserted by nonlinear advection, an increase in dissipation will occur when the advection is positive. This leads to an increase in northward transport of planetary vorticity, and leads to an intensification of the coastal current and an asymmetry in the gyre. As shown shortly, this is borne out by the output from one of the model runs. The model outputs are similar to those of Cox (1981).

4. Results

Wind data over the Arabian sea have been published by Hastenrath and Lamb (1979). Similar data have been published by Cadet and Diehl (1984) for the period 1954–1976. Variations of wind stress off the Somali coast have been described by Bruce (1978), Wylie and Hinton (1982) and by Luther *et al* (1985). Computations of the curl and divergence have been made by Okumu (1985) with a limited data set for the coastal region off east Africa. These data sources were utilized to prepare maps of the curl and divergence for our region of interest. They are shown in figures 1 and 2.

The wind stress was computed from the bulk aerodynamic formula

$$\boldsymbol{\tau} = \rho_a C_D |V_a| \mathbf{V}_a, \tag{20}$$

where ρ_a is the density of air and V_a the wind velocity. We put $\rho_a = 1{\cdot}2$ kg m^{-3} and $C_D = 1{\cdot}25 \times 10^{-3}$. The variation of C_D with wind speed was ignored in the present work. Values of the stress computed by us agreed fairly well with the publications cited earlier. From these values of the wind stress, its divergence was computed (figure 2) numerically by using centred differences.

We chose mean conditions for July because it was a representative month of the monsoon. There is little difference in the monthly mean maps of the wind stress from June to September. The stress pattern begins to stabilize itself from mid-May and remains stable up to the middle of September.

The main features of the curl in July (figure 1) are: (i) high positive values of the east coast of Africa and the coast of Arabia and (ii) strong negative values between

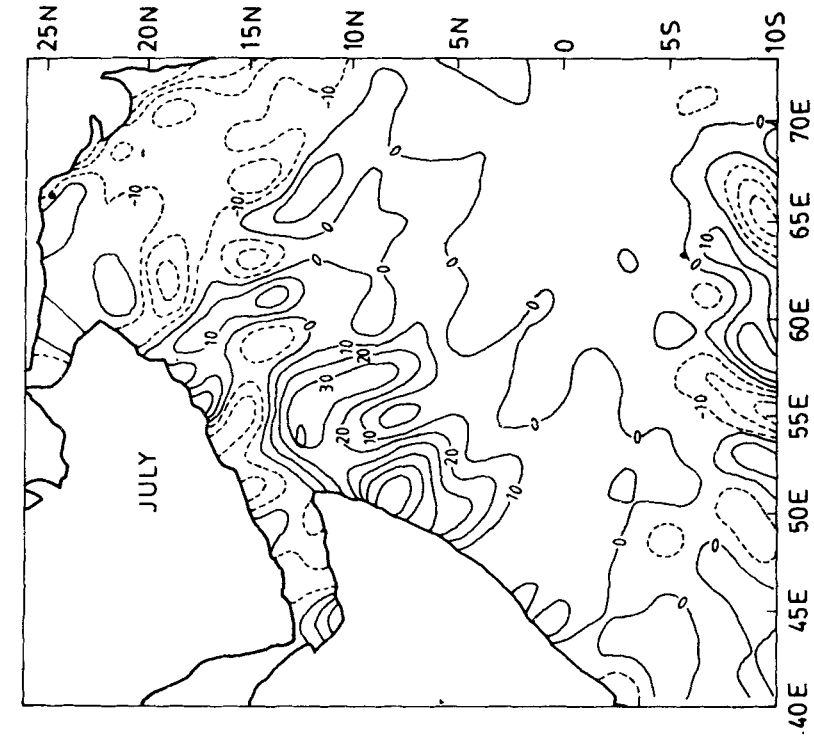

Figure 2. Mean wind stress divergence in July (10^{-8} N/m^3).

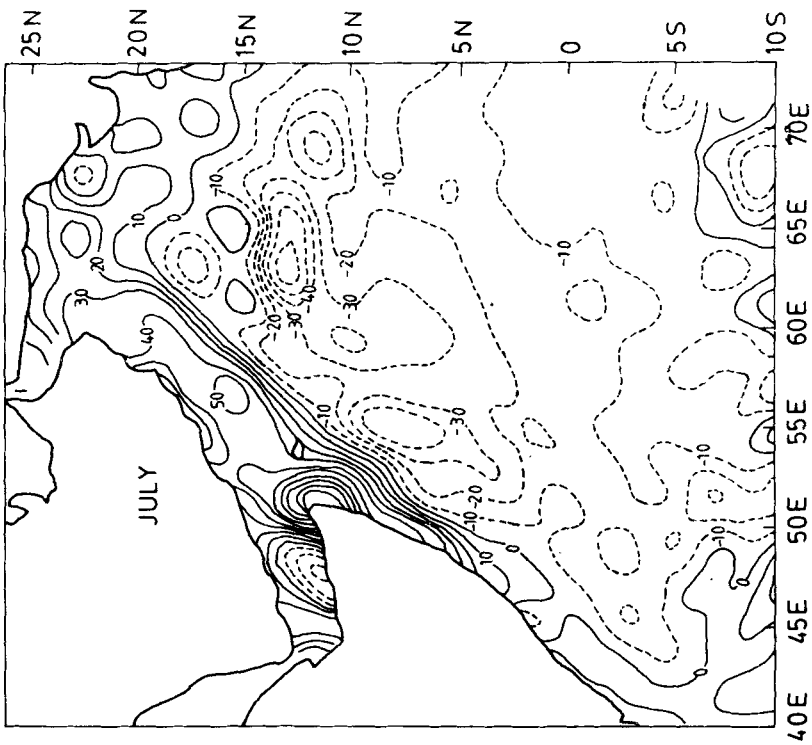

Figure 1. Mean wind stress curl in July (10^{-8} N/m^3).

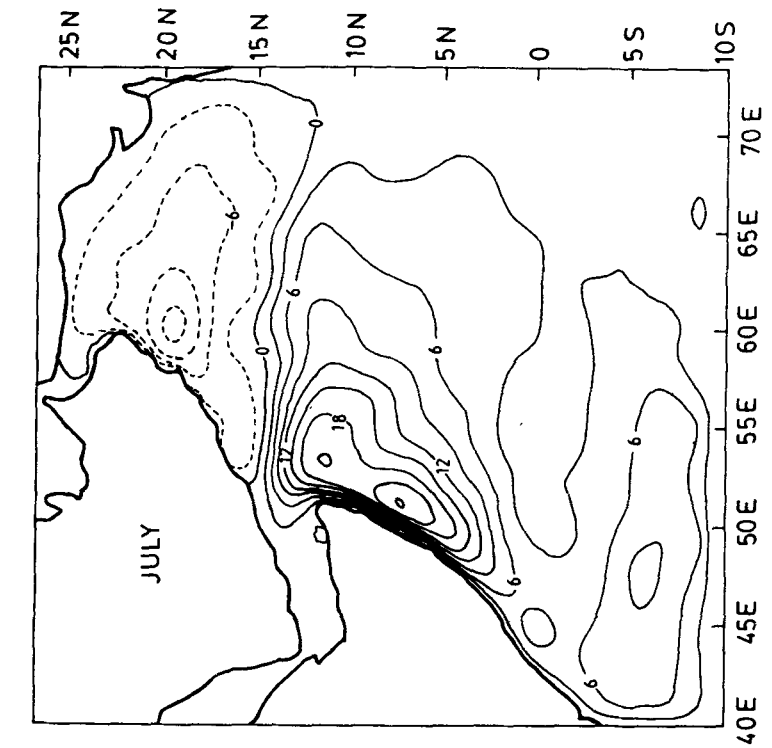

Figure 4. Field of $\psi_1(10^4\,m^2/s)$.

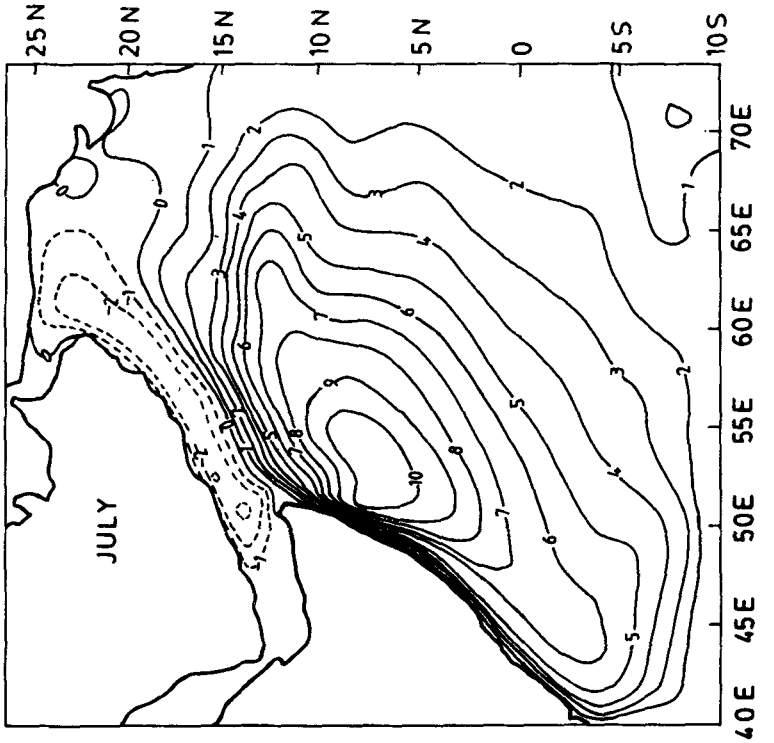

Figure 3. Field of $\psi_0(10^4\,m^2/s)$.

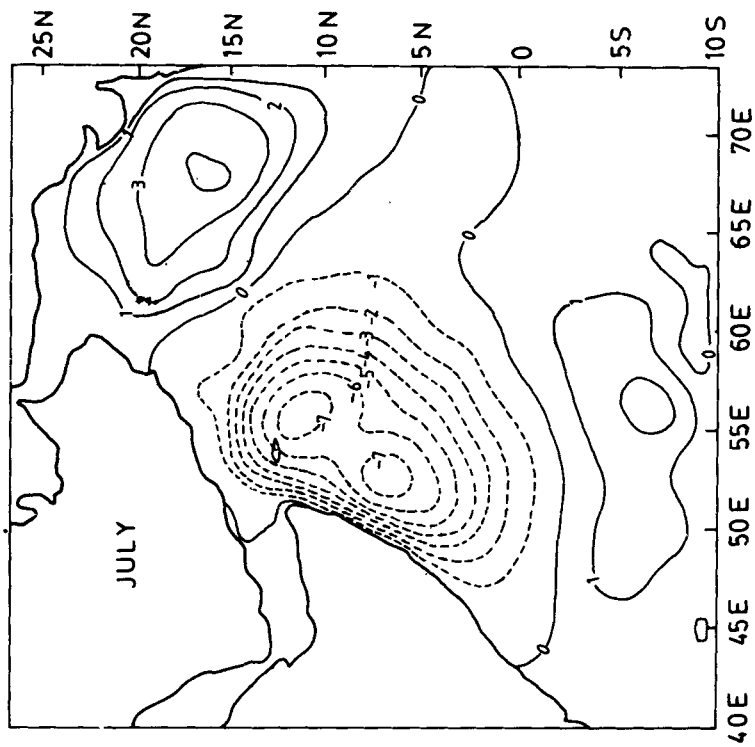

Figure 6. Velocity potential χ_0 (10^4 m^2/s).

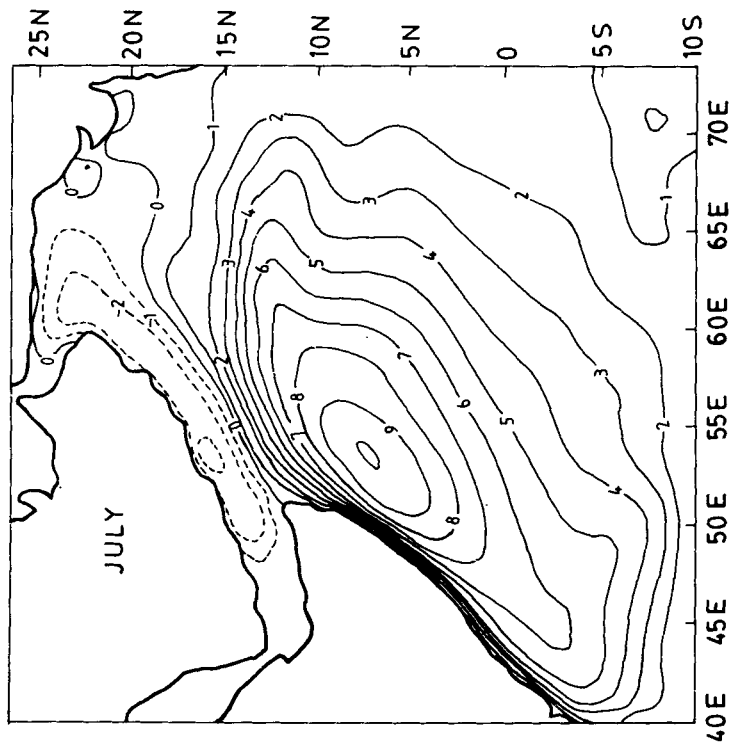

Figure 5. ψ_0 field with nonlinear terms (10^4 m^2/s).

5–15°N and 55–70°E in the interior. Strong upwelling is associated with positive curl, while downwelling occurs over regions of negative curl. Dube *et al* (1986) find that the interior downwelling becomes weak in years of poor monsoon.

The divergence of the wind stress (figure 2) has high positive values in the region between 0–15°N and 50–60°E. Negative divergence prevails between 12–20°N and 60–70°E.

It is interesting to see that the narrow coastal region between 5–12°N is a zone of both positive curl and divergence. This is, therefore, a zone of marked coastal upwelling.

Figures 3 and 4 show the first and second approximations to the streamfunction (ψ_0, ψ_1). As we can see, the inclusion of divergence in the vorticity equation leads to the formation of a second gyre between the equator and 8°S. The second gyre is absent in the first approximation (figure 3), which only shows a big whirl between 5–12°N. The big whirl and the southern gyre is separated by a small eddy.

In figure 5 the streamfunction ψ_0 is shown with the inclusion of the nonlinear term as in (19). The stretching term was not present in this case; consequently, only

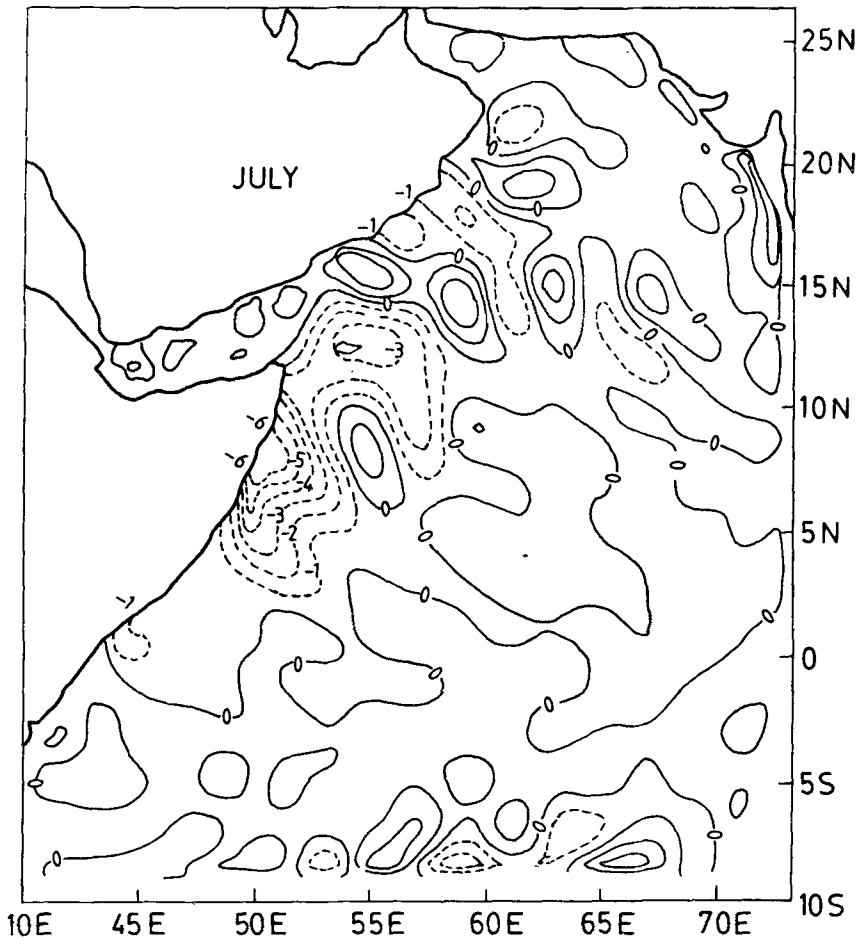

Figure 7. Vertical velocity (10^{-5} m/s).

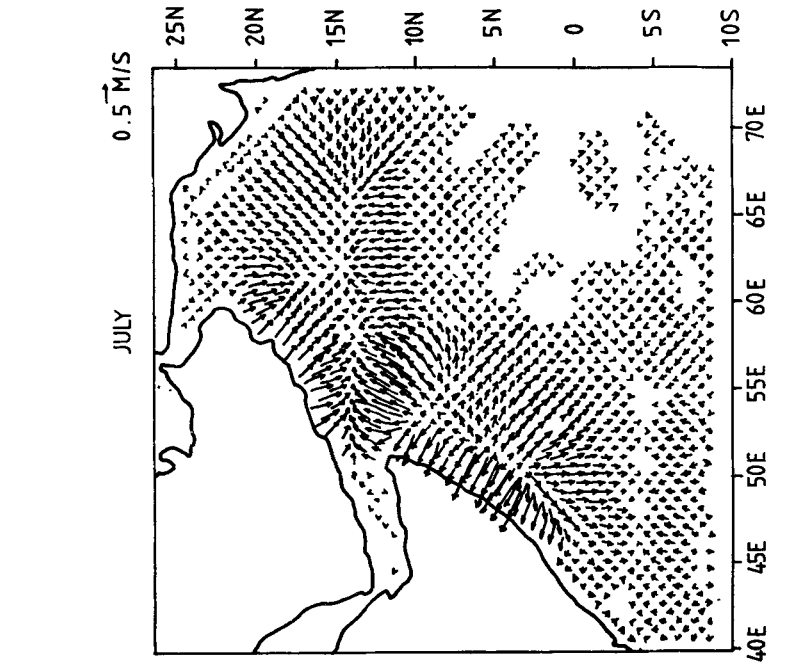

Figure 9. Upper layer velocity (0·5 m/s) from gradients of χ_1.

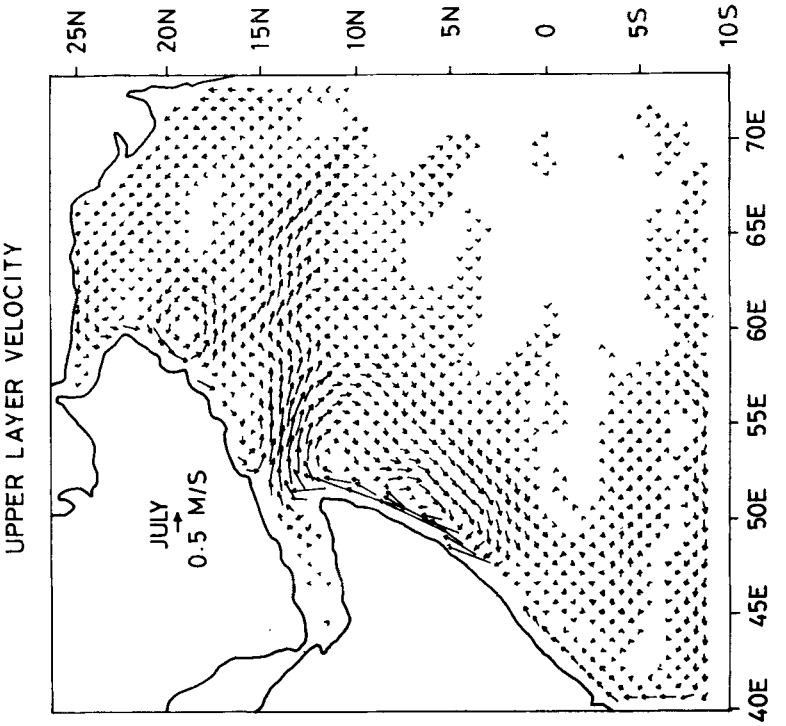

Figure 8. Upper layer velocity (0·5 m/s) computed from gradients of χ_1.

a single gyre resembling the 'great whirl' appears. On the other hand, the coastal current is more intense and the central portion of the whirl near 8°N is considerably distorted. This agrees with our earlier inferences and the results of Cox (1981).

Figure 6 shows the first approximation to the velocity potential X_0. To save space the second approximation X_1 is not shown because there was not much difference between X_0 and X_1. The vertical velocity is shown in figure 7. Strong upwelling off the eastern coast of Africa is the main feature. The intensity of upwelling exceeds the value derived by Luther and O'Brien (1985) by a factor of 3, but there is good agreement on the location of the upwelling zone. Downwelling over the central parts of the Arabian sea is not so prominent.

Figures 8 and 9 show the upper layer velocity on account of rotation ψ_1 and divergence χ_1. It is interesting to note that the strong eastward jet near 12°N is an outcome of the rotational part of the current. This jet carries much of the cooler upwelled waters from the coast to the interior of the Arabian sea. As we see in figure 9, the χ_1 field leads to weak divergent motion over the central Arabian sea.

These figures of the Somali current are interesting because Dube *et al* (1986) suggest that the southern gyre is prominent in a year of good monsoon rain. Our model suggests that the southern gyre is an outcome of the stretching term in the vorticity equation. This, in turn, is related to the divergence of the wind stress.

5. Conclusions

(i) The divergence of the wind stress is comparable to the wind stress curl over equatorial regions of the Arabian sea and the north Indian ocean.
(ii) The southern gyre of the Somali current is an outcome of forcing by the divergence of the wind stress.
(iii) Nonlinear terms in the vorticity equation strengthen the coastal current and introduce an asymmetry in the main gyre.
(iv) A strong eastward jet near 12°N is due to the rotational component of the upper layer velocity. This carries much of the cold upwelled waters from the coast to the interior.
(v) The central parts of the Arabian sea are regions of weak downwelling.

Acknowledgement

The authors thank Dr Brian Johns, University of Reading, U.K. for reading the manuscript and offering valuable suggestions.

References

Bruce J G 1978 Spatial and temporal variation of the wind stress off the Somali coast; *J. Geophys. Res.* **83** 963–967

Cadet D L and Diehl B C 1984 Interannual variability of surface fields over the Indian ocean during recent decades; *Mon. Weather Rev.* **112** 1921–1935

Cox M D 1981 A numerical study of surface cooling processes during summer in the Arabian sea in: *Monsoon dynamics* (eds) M J Lighthill and R P Pearce (Cambridge: University Press) pp. 529–540

Cutler A N and Swallow J C 1984 Surface currents of the Indian ocean; Rep. No. 187, Institute of Oceanographic Sciences, U.K.

Dube S K, Luther M E and O'Brien J J 1986 Relationship between the interannual variability of ocean fields and the wind stress curl over the central Arabian sea and the Indian summer monsoon rainfall (unpublished)

Hastenrath S and Lamb P J 1979 Climatic atlas of the Indian ocean—Part 1: Surface circulation and climate; (Wisconsin: University Press) p. 109

Luther M E and O'Brien J J 1985 A model of the seasonal circulation in the Arabian sea forced by observed winds; *Prog. Oceanogr.* **14** 353–358

Luther M E, O'Brien J J and Meng A H 1985 Morphology of Somali current system during the southwest monsoon in: *Coupled ocean atmosphere models* (ed) J C J Nihoul (Amsterdam: Elsevier) pp. 405–537

Okumu M A 1985 Upwelling and the Somali current, M.S. thesis, University of Nairobi, Kenya

Stommel H 1948 The westward intensification of wind driven ocean currents; *Trans. Am. Geophys. Union* **29** 202–206

Wylie D P and Hinton B B 1982 The wind stress pattern over the Indian ocean during the summer monsoon of 1979; *J. Phys. Oceanogr.* **12** 186–199